EVALUATION OF A HIGH-TORQUE BACKLASH-FREE ROLLER ACTUATOR

Bruce M. Steinetz* and Douglas A. Rohn*

and

William Anderson†

The results are presented herein of a test program that evaluated the stiffness, accuracy, torque ripple, frictional losses, and torque holding capability of a 16:1 ratio, 430 N-m (320 ft-lb) planetary roller drive for a potential space vehicle actuator application. The drive's planet roller supporting structure and bearings were found to be the largest contributors to overall drive compliance, accounting for more than half of the total. In comparison, the traction roller contacts themselves contributed only 9 percent of the drive's compliance based on an experimentally verified stiffness model. The drive exhibited no backlash although 8 arc sec of hysteresis deflection were recorded due to microcreep within the contact under torque load. Because of these load-dependent displacements, some form of feedback control would be required for arc second positioning applications. Torque ripple tests showed the drive to be extremely smooth, actually providing some damping of input torsional oscillations. The drive also demonstrated the ability to hold static torque with drifts of 7 arc sec or less over a 24 hr period at 35 percent of full load.

INTRODUCTION

Roller traction drives have found their way into a variety of industrial applications ranging from low-power, elastomer-coated rollers in paper handling equipment to 100 kW variable-speed pump drives. As power transmissions, few mechanical drives match their low-noise, smooth-torque-transfer characteristics and speed-regulating accuracy. However, their suitability as servodrive mechanisms is just starting to be appreciated. Absence of "backlash" and "cogging" (low-velocity errors) are two notable qualities.

Recent examples include a traction roller servosystem for part positioning on an ultraprecise single-point lathe (ref. 1) and an advanced technology propeller pitch control mechanism (PCM) for future large turboprop aircraft

*NASA Lewis Research Center, Cleveland, Ohio.
†Nastec, Inc., Cleveland, Ohio.

(ref. 2). The traction feed system built by Lawrence Livermore Laboratories, which used a drive roller against a translating traction bar, had a positioning repeatability of 0.005 μm (0.2 μin.) under thrust loads to 1300 N (300 lb) using laser interferometry feedback (ref. 1).

A promising approach for meeting the demanding PCM requirement is an all electromechanical system incorporating a multiroller 210:1 hybrid traction drive for a Mach 0.8, 150 passenger turboprop commuter aircraft (ref. 2). This torsionally stiff system can vary the pitch of 4 m diameter propellers carrying up to 10 000 kW. With the proposed low-friction mechanism coupled to a high-resolution digital controller, blade position accuracies of better than 3 arc min of a degree are projected, well within synchrophasing (precise speed control) allowances of a multiengine aircraft of this size. This 1500 N-m (1100 ft-lb) actuator would also be suitable for other high torque applications such as tank turret aiming and missile tracking mechanisms.

In this investigation, a 16:1 ratio, 430 N-m (320 ft-lb) output torque roller actuator (fig. 1) was evaluated experimentally to determine its potential suitability as a space vehicle, high-torque actuator, such as for a control moment gyro (CMG) gimbal drive. Analytical predictions of the torsional stiffness of the drive are compared with static torsional stiffness measurements. Data on the drive's zero backlash, torque ripple, starting friction, and hysteresis characteristics were also obtained as well as data on its positional accuracy performance and ability to attenuate some drive system torque ripples.

BACKGROUND

Traction drives in their simplest form are just two smooth, unequal-size wheels in driving contact. As a minimum, a preload system is required to maintain sufficient normal load to prevent the rollers from slipping over one another. Drives can be designed with either a fixed or variable preload depending on the particular application. Unlike gear meshes, the roller contact due to its low sliding nature can be designed to operate for extended time periods without liquid or grease lubrication for low-power applications. This can be accomplished by either using high-traction solid-film coatings such as ion-plated gold or silver or using advanced, low-wear, high-traction polymers such as certain polyimides or polyamide-imides. The elimination of depletable liquid lubrication is a decided benefit for spacecraft mechanism applications.

Furthermore, rollers, unlike gears, have the ability to slip harmlessly at predetermined traction limits. This overtorque, release-clutch tendency can prevent catastrophic damage if jamming should occur at some point in the mechanism drivetrain.

Light-duty (up to about 10 kW) variable ratio traction drives have been commercially successful in industrial applications for many years. Due to their inherent smooth torque transfer characteristics and potential for cost

reductions, traction drives have been investigated as replacements for geared drives for fixed ratio power transmissions and mechanisms.

Unlike a simple gear mesh, the normal load imposed on a traction contact must be several times higher than the transmitted traction force to prevent slip. Thus, to achieve high-power (or torque) density, the traction drive should be constructed with multiple, load-sharing roller elements which can reduce the contact unit loading. Planetary roller drives have multiple contacts and ensure that the normal contact loads are reacted internally by the ring roller rather than by bearings. However, because of planet roller-to-roller interference, a single row planetary drive is limited in speed ratio.

The drive system devised by A.L. Nasvytis in the early 1960's (ref. 3) used the sun and ring-roller of contemporary planetary traction drives but replaced the single-row of equal diameter planet rollers with two or more "stepped" or dual diameter planets. With this new multiroller arrangement, practical speed ratios of up to 250:1 could be obtained in a single stage with three planet rows. Furthermore, the number of planets carrying the load in parallel could be greatly increased for a given ratio. This resulted in a significant reduction in individual roller contact loading with a corresponding improvement in torque capacity. The Nasvytis type drive evaluated herein achieves a 16:1 ratio in a single stage using two rows of stepped planet rollers (fig. 1).

A novel geometric arrangement that combines traction rollers with gears in parallel was also devised by Nasvytis (ref. 3). In the roller-gear drive, as it is termed, the center portion of the roller is replaced with a spur gear. The rollers not only serve to transmit a portion of the torque but also provide a support bearing function since their diameters are equal to the pitch diameter of the gear. The rollers which share torque in parallel with the gears eliminate the effects of backlash and help minimize breakaway torque while adding substantial stiffness to the drive system.

The performance of a 26:1 ratio, 540 N-m (400 ft-lb) CMG rotary actuator, which incorporated a roller-gear drive (fig. 2) in combination with a brushless dc motor, was evaluated in reference 4. In this drive, the rollers share 25 percent of the torque in parallel with the gears. Static output torsional stiffness values of 680×10^3 N-m/rad (500×10^3 ft-lb/rad) or greater were measured at the zero torque crossing point. Breakaway or starting friction varied from 0.4 to 2.5 percent of rated torque. While no backlash was detected, a small degree of lost motion (hysteresis) was measured that ranged from 2.9 to 4.7 arc sec up to 25 percent of maximum torque. Tests of a similar, but smaller, 106 N-m (78 ft-lb) torque, 15:1 ratio roller-gear/brushless dc motor servodrive were conducted in reference 5.

ACTUATOR DESIGN

Specifications

The need for a backlash-free, high-torque, low-torque ripple actuator was identified for a large space vehicle application. Critical system requirements included a minimum drive torsional stiffness of 340 000 N-m/rad (250 000 ft-lb/rad) at the output, a low weight, and a minimum design life of 1600 hr. Maximizing the drive's torsional stiffness while minimizing the drive weight consistent with the achievement of required life were the paramount considerations guiding the design. Structural design tradeoffs and material selections were consistent with flight hardware requirements.

Maximum input speed to the drive is 275 rpm and maximum input torque is 27 N-m (20 ft-lb), which is equivalent to 0.78 kW (1.05 hp). These conditions exist only when the actuator must reposition its driven element from point A to point B, which is only 6 percent of the total duty cycle. Most of the time the mechanism is hunting or "dithering" around a desired set point.

Two drive designs were generated, one based on lubrication with a high-traction vacuum oil and one based on dry operation. The overall configuration and dimensions were identical except for the preload mechanism which provided higher normal loads in the wet drive to transmit the same torque with a 40 percent less available traction coefficient. The rolling-contact fatigue life of the lubricated drive was well in excess of the required 1600 hr. Since dry lubrication has advantages in space, the dry configuration was chosen for evaluation.

This drive was designed to operate without liquid lubrication with a design traction coefficient of 0.1, 20 to 100 percent below the maximum available traction coefficient of the gold-ion-plated sun rollers against their mating steel first-row planet rollers (ref. 6). Gold was ion plated onto the sun roller surface with a thickness of 0.2 μm (7.8 μin.) as a dry film lubricant between the sun and first-row planet contact to prevent the rollers from cold welding in the vacuum environment. Life limitation in this design is one of wear of the gold layer. Based on sliding friction data (ref. 7), the gold thickness was determined for a minimum 1600 hr of operation.

Geometry

The drive is nominally 25 cm (9.84 in.) in diameter by 22 cm (8.66 in.) in length and weighs 10 kg (22.1 lb) (fig. 1). This compact Nasvytis planetary drive packages well in the tight required design envelope. The servomotor-driven input shaft transmits torque to the two halves of the sun roller through two sets of torque loader balls. The sun roller, in turn, drives five stepped first-row planets which are in contact with five second-row planets. These outer planets carry the torque to the ring roller attached to the output shaft. Because of the double end geometry of the rollers, ten, twenty, and ten parallel contact paths occur, respectively, at successive contacts. The number of

planet rollers per row, number of rows, and relative step sizes are design parameters to be optimized for a given application.

The torque loading mechanism increases the normal load between rollers in direct proportion to the applied torque. The potential for slip is not only eliminated by incorporating a roller loading mechanism, but also the normal loads on the rollers do not have to be set at maximum at all times. Thus, the system's fatigue (wet lubricated drive) or wear (dry drive) life is extended and frictional losses are minimized.

The torque loading mechanism consists of six 0.64 cm (1/4 in.) diameter balls contained in ramp-shaped pockets equally spaced circumferentially between the sun roller flanges and thrust collars. The sun roller surfaces are crowned cones that mate with the first-row planet rollers with their slightly conical (4°) surfaces. When torque is applied to the drive above some predetermined preload setting (ranging from 10 to 50 percent of maximum torque), the sun roller thrust collars will advance circumferentially relative to the sun roller flanges. This will cause the balls to roll up their ramps, squeezing the two sun roller halves together axially. The axial clamping force, in turn, produces a radial loading on the roller cluster through the sun's tapered contact with the first row planets. The two sun halves are synchronized to move together by means of a series of interlocking fingers on each roller. The ratio of tangential force to normal force imposed on the traction drive contacts for a given torque; in other words, the applied traction coefficient can be varied by simply changing the slope of the ramp-shaped pockets. This applied traction coefficient is always designed to be less (at least 20 percent less in this case) than the maximum available traction coefficient to provide sufficient safety margin against slip.

TRACTION DRIVE ANALYSIS

Torsional Stiffness

High drive actuator system torsional stiffness is generally important for a variety of reasons. The most important reason for this application was to increase the system's bandwidth (response rate limited by natural system resonance). To achieve high bandwidth, the design philosophy was to make each structural/traction element as stiff as possible while minimizing rotational inertias (J_{Drive} = 0.055 kg-m^2 at output) consistent with the other requirements of the drive. The requirement for high torsional stiffness had the greatest influence on the design of the torque loader, the second-row planet bearings, and the spider cage/roller support housing. The torque loader system was integrated in the sun roller instead of at the optional ring roller position, since the effective Hertzian compliance of the loading balls is significantly reduced by the square of the drive speed ratio.

Cylindrical roller bearings modified to essentially zero-mounted radial clearance (less than 2.5 μm (0.0001 in.)) were used as second-row planet support bearings rather than ball bearings. The aluminum spider cage/roller support housing was fabricated from a solid piece with cutouts for the second

planets rather than a bolted-up structure that could sacrifice stiffness at the connections.

The components within the drive which contribute to stiffness (or its reciprocal, compliance) were analyzed. The main contributors included the spider cage, planet bearings, input shaft and torque loader system, roller support housing backing plate, traction contacts, outer housing, bearing post depression in backing plate, and the output shaft. In analyzing each of these components it should be noted that their individual stiffness values must be adjusted by the appropriate speed ratio factor to relate their contribution to an effective overall torsional stiffness of the drive, typically (in this paper) at the output shaft.

The predicted effective stiffnesses at the low-speed shaft of each major drive component are listed in table I at zero torque (startup) with an initial contact preload set at 50 percent of maximum. This zero torque stiffness is critical to the response rate of a positioning mechanism that continuously adjusts about a new set point. The components have been ranked according to their percent of compliance contribution, which helps to identify the components that require the most improvement for maximum drive stiffness. The maximum available traction coefficient between the gold sun and steel first row planet contacts was conservatively assumed to be $\mu = 0.12$, and the maximum available traction coefficient for all remaining steel components was conservatively taken as $\mu = 0.2$. The overall predicted output shaft torsional stiffness was initially 670 000 N-m/rad (490 000 ft-lb/rad).

Compliance calculations for the input shaft and torque loader system, outer housing bearing post depression in backing plate, and output shaft were idealized and treated with a normal strength of materials approach. The spider cage was modeled as a repeated frame structure of aluminum support and steel bearing posts connected by a rigid link, the carrier ring, pinned to their ends (ref. 8). The cylindrical roller bearings were modeled with a 5 μm (0.0002 in.) diametral clearance using the method of reference 9. The roller support housing backing plate for the planet bearing posts was modeled as a disk with torque applied at the inside diameter and reacted at the outside diameter as described in reference 10. The traction contacts were analyzed using the comprehensive technique developed in reference 11; this technique is summarized in the appendix. A computer program, which was written using this approach, calculates traction contact compliances at each of the roller contacts and relates them to the output shaft. The roller contacts theoretically contribute only 9 percent of the drive's compliance (see table I).

When the component stiffnesses k_i are expressed as equivalents at the output shaft, the components can be treated as torsional springs in series. The total stiffness $K_{T,Drive}$ is given by

$$K_{T,Drive} = \left(\sum_{i}^{n} k_i^{-1} \right)^{-1}$$

Other Considerations

Traction roller contacts can have a broad variety of available maximum traction coefficients, normal loads, contact ellipticity ratios, and applied loading. The relative effects of these variables are important to the designer of a traction drive mechanism that requires a certain level of torsional stiffness. For a given application, usually defined in terms of driven torque load and overall ratio requirement, each parameter described in the appendix can be adjusted, though not totally independently, to achieve the desired stiffness. Holding other parameters constant contact torsional stiffness increases with an increase in normal load and available traction coefficient but decreases with an increase in transmitted traction force. Large variations in stiffness can be achieved through the choice of roller-contact geometry. Contacts with a high ellipticity ratio (wide in the direction perpendicular to rolling) have higher stiffnesses. Roller size has the strongest stiffness effect, as shown in reference 11, if just static windup without rolling contributions is considered. In general, contact stiffness k_t is related to tangential force F_x, normal load N, ellipticity ratio a/b, maximum available traction coefficient μ, torque T, and the ratio F_x/N as follows:

$$k_t \propto (\text{size})^{7/3} \quad \text{at constant} \quad F_x,\ N,\ a/b,\ \text{and}\ \mu$$

$$k_t \propto (\text{size})^{2} \quad \text{at constant} \quad T, F_x/N,\ a/b,\ \text{and}\ \mu$$

The foregoing cases show that contact torsional stiffness will approximately double for a 40 percent increase in roller sizes.

Roller coating effects. - In the roller actuator reported herein, the sun roller was ion plated with a 0.2 μm coating of gold to provide protection against wear and cold welding of the steel rollers in a vacuum. The effects this roller coating had on torsional deflections were determined using the analysis of reference 12. In that study, it was shown for a specific pair of steel rollers that a 30 percent increase in deflection over noncoated rollers would result with a 2.5 μm coating of material (having an elastic modulus 100 times less than steel) under a static traction force one-fifth the normal load. For the roller drive evaluated in this investigation, the gold coating was thinner (less than one-tenth the thickness of the previous case) with an elastic modulus much higher (one-third instead of one-hundredth that of steel) under a static traction force one-tenth the normal load. Thus, it was concluded that the gold coating had a negligible effect on torsional stiffness. It should be noted that the stiffness of a roller mechanism design with a relatively thick polymer or elastomer coating would probably be less than with a gold coating.

Ratio effects. - Static torsional stiffness is also dependent on the ratio of the drive and number of planets as shown in figure 3. This plot was generated for a simple, single-row planetary roller drive having the sun as input and ring as output. Suitable ring diameter and input shaft, output shaft, planet bearing and support structure stiffnesses were chosen for a maximum output torque of 170 N-m (1500 in.-lb). For this plot, output torque, ring diameter, contact ellipticity, available and applied traction coefficients,

input shaft stiffness, and output shaft stiffness were held constant. For a simple planetary, there exists a maximum ratio for each number of planet rollers without planet roller-to-roller interference. Also, there is a practical limit to speed ratio (approximately 7) in a simple planetary above which the size of the sun roller relative to the ring roller becomes so small as to unfavorably overload the sun roller contact for appreciable torque transfer.

In general, effective stiffness increases most rapidly with ratio when planet bearings and support posts are stiff (upper set of curves in fig. 3). This is because the input shaft stiffness becomes more dominant (proportional to ratio squared at output) when the bearings and supports are stiff. Thus, in maximizing drive stiffness or comparing drives of different stiffnesses, ratio, individual component stiffnesses, and sizes must all be considered.

Comparison with gears. - A comparison of the theoretical stiffness of equally sized gear and traction roller pairs made of steel showed that traction contacts were typically two or three times stiffer than gears under comparable loads (ref. 13). Figure 4 shows the stiffness of traction contacts relative to comparably sized and loaded gears plotted as a function of gear tooth size (diametral pitch). The method used to analyze gear stiffness considers the local Hertzian normal compliance and tooth beam bending. It also considers standard undercut and fillet bending and shear as well as foundation flexibility (ref. 14).

It is apparent from figure 4 that gear mesh stiffness is relatively insensitive to the number of teeth (diametral pitch) or the torque level and that fluctuations between two relatively discrete levels occur as the load is transferred between single-tooth and double-tooth contact. This stiffness fluctuation contributes to velocity fluctuations in a loaded gear train, in addition to fluctuations from normal geometric tooth (unloaded) errors. In contrast, the stiffness of a traction drive contact is essentially constant for a given load, although some degradation with increased transmitted torque will occur as shown.

RESULTS AND DISCUSSION

Verification of Compliance Model

Simple contact rig. - Data that can verify a compliance analysis of torsionally strained contacts are few in the literature. To corroborate the analysis used, tests on a simple configuration were conducted at NASA Lewis Research Center. The apparatus used consisted of a 7.6 cm (3.0 in.) diameter crowned roller loaded against a flat (0.05 μm surface finish) plate (see sketch in fig. 5). Normal loads up to 4450 N (1000 lb) could be applied by spherical roller bearings on the roller's support shaft. Torque was applied to the shaft by an arm and weight system. Linear displacement probes and dial indicators measured the circumferential deflections of an arm fixed to the roller. Preliminary compliance measurements showed that test rig flexibility had to be measured and subtracted from the deflections of the traction roller.

Contact stiffness. - Comparison of predicted and measured compliance for the roller/plate contact is shown in figure 5 for a normal load of 4450 N (1000 lb). The slope and thus the roller contact stiffness of the data agree well with the theoretical predictions. Stiffness is relatively constant up to the normal maximum torque operating limit set by the normal loading mechanism. Of course, without an autoloading mechanism, stiffness dramatically drops as the slip torque is reached as indicated by both the data and the theoretical model. The 5 to 6 arc sec scatter between the data and the theory in the mid-torque region is believed to be due to a presently unaccounted for nonlinearity in rig flexibility at the arc second level.

Roller Actuator Stiffness

Test setup. - Static torsional stiffness measurements of the drive with the sun roller (input) locked and torque applied to the output shaft were performed. Torque was applied to the transmission through a calibrated torque meter using a smooth hydraulic piston loading system. Angular displacements of the output shaft were measured using an eddy-current proximity transducer mounted at a 14 cm (5.5 in.) radius. The effects of rig mounting flange flexibilities were minimized by mounting the position transducer directly to the housing mounting flange. Output shaft displacements were corrected electronically for small windups noticed at the input shaft using a second eddy-current probe mounted at the input shaft. On the average this correction amounted to only 4 percent of the output shaft rotation. The angular resolution of the measurement system was 1.9 arc sec. Output shaft torque and angular deflection traces were recorded on an x-y chart recorder revealing drive stiffnesses and hysteresis.

Experimental results. - The torque-angular deflection trace of the drive preloaded to 50 percent rated torque capacity (fixed at the sun shaft) is shown in figure 6. These traces were obtained by repeatedly cycling (2 cycles shown in figure) over positive and negative torque values. Inelastic displacements from contact microslip resulted in some hysteretic (microslip) loss during torque reversals. However, the slope of the torque-angular deflection curve is constant across the zero torque line, thus indicating no "backlash" is present. Backlash would appear in this trace as a horizontal or "zero stiffness" line. This inherent, backlash-free behavior of traction rollers is a decided benefit for mechanism control systems that typically must position a load around a desired set point.

Torsional stiffness was graphically determined from the torque-angular deflection trace at the zero torque crossing point and was found to be 230 000 N-m/rad (170 000 ft-lb/rad) ±10 000 N-m/rad. This is roughly one-third the initial predicted value. Drive stiffness was relatively constant with applied torque for the 50 percent preload case up to 40 percent design torque. However, a significant loss in stiffness occurs at torques above the preload setting due to rotation of the loading mechanism. This is normally not a serious problem with most positioning mechanisms since stiffness at the torque crossing is most critical. Stiffnesses with drive roller normal loads set to 75,

100, and 125 percent rated torque capacity were found to be 210 000, 240 000, and 250 000 N-m/rad, respectively.

Individual stiffness measurements of key drive components were made to investigate the discrepancy between the measured and predicted drive system stiffnesses. The two largest contributors to drive compliance are the spider cage support structure and the second-row planet support bearings. In conducting each of these tests, loading conditions were imposed which closely duplicated those in the drive. The stiffness of the spider cage was measured while installed in the drive by measuring the angular deflection of the spider cage about the center line of the drive using a similar eddy-current probe setup as described earlier. The measured linear stiffness reflected to the output shaft was 990 000 N-m/rad (730 000 ft-lb/rad), approximately half that predicted analytically using the simple beam model. Evidently, a detailed finite element model would be needed to provide better stiffness estimates for the relatively complicated spider cage (see fig. 1).

Radial stiffness measurements of four of the drive's cylindrical roller planet bearings were made in a specially designed loading fixture with the same setup that exists in the second-row planet rollers. Two bearings were loaded in tandem with a calibrated test machine fixture (fig. 7). Displacement measurements were made of the inner race relative to the outer race with a differential electronic indicator system with a resolution of 0.1 μm (5 μin.). Data for one of the bearing tests, typical of the load-dependent stiffnesses for each of the four bearings tested, are shown in figure 8. Comparing these data to those predicted by theory of reference 9, assuming a nominal 5 μm (0.0002 in.) diametral clearance shows a significant difference in the slopes or radial stiffnesses near zero load. The measured radial stiffness is approximately 30 percent of that predicted near zero load, approaching 60 percent of the predicted value at higher radial loads. The test data reveal a "settling-in" region as the load is first applied; this behavior is not reflected by the bearing deflection model.

The measured stiffnesses of the bearings and the spider cage were much less than the initial predictions indicating areas where drive stiffness was sacrificed. For comparison purposes, the measured stiffnesses of these two components were used in place of their original predictions (table II) to recalculate an overall predicted drive stiffness at zero-torque load. This stiffness of 370 000 N-m/rad (270 000 ft-lb/rad) is now 60 percent higher than that measured for the drive system.

When analyzing the contribution of the planet bearings to drive stiffness, both theoretically and using actual bearing data, it was assumed that all planet bearing supports shared the load equally. Due to manufacturing tolerances for bearing post locations, the bearings on the test drive are likely to be out of perfect position. Thus, at initial load application only one or two of the supports may be, in fact, loaded. In view of this nonideal load sharing, a decrease in the effective planet bearing system stiffness would be expected. For instance, if it were assumed that only two of the five bearing supports were active at the initially applied torques, then the effective bearing support compliance would increase by a factor of 2.5, resulting

in a recalculated drive stiffness of 230 000 N-m/rad (170 000 ft-lb/rad). This stiffness agrees exactly with that measured.

It is clear that structural component and bearing compliance dominate the overall stiffness of the drive. Even doubling or tripling compliance of the traction drive contacts themselves would be expected to have only a relatively minor overall effect.

Based on these results, drive stiffness improvements resulting from a redesign of the second-row planet support structure were analytically considered. Machining the spider cage from beryllium with more rigid connections for planet bearing posts would be expected to improve this component stiffness by 90 percent. Using preloaded or line-to-line fit cylindrical roller bearings would remove the initial "settling in" behavior observed in the bearing radial stiffness measurements, giving appreciable higher stiffness at zero load (zero drive torque).

Torque Ripple/Breakaway Torque

Apparatus. - Tests were conducted to determine (approximately) the torsional ripple/attenuation characteristics of the roller actuator. A variable-speed dc motor drove the high-speed shaft of the actuator. Steady torsional loads were applied to the output shaft through a pulley/weight system by lifting dead weights. The steady-state (or dc) component as well as the fluctuating (or ac) component input and output torque signals were measured using torque meters and were recorded on a strip chart recorder. The roller actuator normal loads were set for 50 percent maximum torque capacity. System calibration was required because of unavoidable torsional ripples caused by the variable-speed motor input and a mild resonant vibration on the cable-mass system at about 4 Hz. Calibration was carried out using a "dummy" shaft directly coupled between the input and output torque meters with the roller drive removed.

Torque ripple test results. - The variations of roller actuator input and output torque signatures for one complete output shaft revolution are shown in figure 9. The actuator was driven at 10 and 20 percent of maximum speed and at three torque levels corresponding to 15, 25, and 31 percent of maximum torque at 50 percent preload. Data for both input and output torque are presented with the ripple shown as a percent variation (plus/minus) of the noted steady-state torque for the 10 percent speed case. Data collected at 20 percent speed showed virtually the same trends. The figure shows that the input torque varied approximately 7 to 8 percent while the output torque varied on the order of 0.3 percent. If no attenuation (damping) was present, then input and output torque percent fluctuations would be expected to be about the same. This suggests that the drive does not excite or amplify torsional oscillations but, in fact, helps to attenuate vibration through Coulombic damping. The traces appearing in figure 9 were taken with prerun rollers having less than perfect surface condition. Thus, these traces are considered to represent a conservative view of the smooth torque transmitting capability of the test drive.

In contrast, gearing must be of high precision to minimize the torque ripple produced by kinematic errors from inherent tooth spacing inaccuracies and flexible tooth bending under load. However, even very precise gears will produce some meshing excitations as the transmitted load is passed from single tooth to double tooth contact and back.

Breakaway torque. - Static frictional torque, or the minimum torque applied to the input shaft necessary to rotate the drive without any load, was measured for various drive preload settings early in the test program. This relatively small breakaway torque is present at any drive speed and makes up a part of the rolling power losses. Breakaway torques at the input ranged from 12 oz-in. at 35 percent preload to 21 oz-in. at 56 percent preload. For all of the measured preload settings up to 100 percent, breakaway torques were less than 1.9 percent of maximum allowable torque. A tradeoff between low breakaway torque and loss in stiffness due to loading mechanism travel must be made by the designer in setting the proper preload.

Positional Accuracy

Apparatus. - A simple test was devised to determine the positional accuracy of the test drive under load in an open-loop control mode. Tests were conducted by driving the input precisely 64 revolutions under four steady torque load levels by raising a weight at a constant speed. The system was then "unwound" by rotating the input shaft back to its initial position while maintaining torque in the same direction. Accuracy measurements in terms of the difference in output shaft angular position before and after rotation were made using a micrometer/lever arm system that could easily resolve angular positions to within 8 arc sec of a degree. Starting and ending positions of the input shaft were precisely reregistered using an indexing arm that contacted against a precision machined surface.

Accuracy results. - Data collected for average angular positional error shown as a percentage of total rotation are given for various output torque loads in figure 10. The percent angular positional errors of the output shaft were calculated by dividing the difference between output shaft starting and ending positions by the four revolutions made. As shown in figure 10, the angular error increased with applied torque load ranging from 0.08 percent under 5 percent load to a maximum of 0.98 percent at 31 percent of maximum allowable torque while drive normal loads were set at 50 percent of the maximum value.

These small errors in reproducing commanded input position are caused by two unavoidable characteristics of roller drives. The phenomenon of rolling creep under torque loads is the major contributor to open-loop positional inaccuracy. As each pair of rollers roll over each other under a steady torque, there is a small relative speed difference which is seen at the output as lost motion. The creep or positional error shown in figure 10 increases with torque as predicted by equations (2) and (4) of the appendix. At low torques, or when the drive operates unloaded, very small kinematic errors due to imperfectly ground rollers (diameter tolerance, out-of-roundness, lobing,

waviness, etc.) can be present. Hence, for critical point-to-point (PTP) positioning applications the control system must be closed loop in order to feedback output position when using roller actuators. This is not uncommon for such precision positioning mechanisms.

Long-Term Holding Ability

In some critical mechanism applications, the ability to position and then hold a load in that fixed position without a brake mechanism is a decided benefit. Though not a critical design requirement of the roller actuator, the drive's long-term holding ability was tested for three steady torques (25, 50, and 70 percent maximum design torque) using the same loading and measurement systems as described in the Roller Actuator Stiffness section. Drive roller normal loads were set at 75 percent of maximum. Total drive output shaft rotation was measured for 24 hr with the input shaft locked (fig. 11). Initial drive torsional windup due to load application is shown at time zero.

The additional rotation (drift) shown is mainly attributed to the tangential, time-dependent yielding or plastic creep of the heaviest loaded interlocking surface asperities. This deformation, greatest just after startup, asymptotically approaches a steady-state value as stress-strain equilibrium is reached.

SUMMARY AND CONCLUSIONS

Operating characteristic tests were conducted on a high-torque roller drive suitable for a space vehicle actuator application. Analysis and test results are presented for a 16:1 ratio 430 N-m (320 ft-lb) output torque drive having two rows of stepped planet rollers. This drive operates without liquid lubrication using traction rollers ion plated with 0.2 μm of gold. Estimated service life for the prescribed duty cycle is at least 1600 hr for this thickness of gold. The drive is nominally 25 cm in diameter by 22 cm in length and weighs 10 kg. The output torsional stiffness of the drive was measured by torsionally loading the output shaft while the input shaft was locked. Theoretical calculations of the drive's torsional stiffness were made and agreed within 60 percent of the measurements at low torque when including the effect of the measured compliance of the second-row planet support structure and bearings. The method of calculating traction contact torsional stiffness as a function of normal load, applied traction force, and roller dimensions among other variables was reviewed. Torsional ripple tests were conducted at 10 and 20 percent speed for torques up to 31 percent of allowed torque at 50 percent fixed preload. Open-loop positional accuracy of the drive's output shaft was also measured as a percent error of total rotation as a function of driven torque. Based on these findings, the following results were obtained:

1. Planet bearings and support structure cause the greatest loss in drive stiffness, accounting for more than 50 percent of total.

2. Traction contacts are very stiff contributing just 9 percent to system compliance based on an experimentally verified traction compliance model.

3. Drive exhibited zero backlash but displayed a small hysteresis displacement of 8 arc sec.

4. Torque ripple was extremely small. Coulombic damping attenuated torque oscillations from 7 to 8 percent at input to 0.3 percent at output.

5. Open-loop positional accuracy of drive degraded with transmitted torque. A closed-loop control system is needed for arc second positioning applications.

6. Drive demonstrated ability to hold torque for extended periods of time with drifts in position of the order of arc seconds.

- APPENDIX -

CONTACT TORSIONAL STIFFNESS ANALYSIS

When two elastic bodies, such as traction rollers, are brought into contact and loaded under a system of forces, deflections occur. When the load is a normal force, the deformation and contact area are given by the classical theory of Hertz. Adding a tangential force produces a relative deflection of the bodies in the tangential direction. A magnified cross-sectional view of the contacting bodies under these conditions is shown in figure 12. If the bodies are rollers or balls which are allowed to rotate under these forces, fresh unstrained material passes through the effective contact region which increases the relative displacement of the bodies. The analysis of reference 11 as it relates to traction roller contacts will be briefly reviewed herein.

Analytically, contact compliance is treated as a boundary value problem in elasticity with several conditions to be satisfied. In simplified terms, the first constraint is that the addition of a tangential force to the contact does not alter the Hertzian normal pressure distribution. Second, all the assumptions inherent to the Hertzian solution are retained, including nonwarping of the contact surface, bodies not too closely conforming in the contact area, body radii large in comparison with contact dimensions, and like elastic properties of the two bodies. Third, the contact region is divided into two zones: one with "microslip" or relative motion between the mating surfaces, and one where the two surfaces are "locked" together. In the slip region, the applied shear stress (traction force per unit area) is assumed to reach its limiting value, proportional to a constant traction coefficient μ times the local normal pressure in accordance with Coulombic fiction. Within the locked region, the applied shear stress is less than μ times the normal pressure. Outside the Hertzian contact area, traction is zero. The local deflection of a point on the surface with respect to a distant point in the body is constant over the locked region and varies over the slip region and outside the contact area. Far away from the contact, the strain is zero.

These considerations apply equally to two cases: static loading and rolling under an applied tangential load. Deformation in a steady rolling contact is viewed from a stationary coordinate system with the origin at the center of contact. Material of each contacting body flows through the contact region under a strain field which is invariant with time. The static case, which is static only in the sense there is no rolling (forces and deflection can vary with time), consists of torquing two contacting rollers and allowing only the motion due to contact compliance to occur.

Static Roller Compliance

For a pair of contacting static rollers under equal and opposite normal loads and proportional and opposite torque loads, the static torsional compliance C_t of <u>one</u> roller was found in reference 11 to be

$$C_t = \frac{1}{2\pi G a r^2}\left(1 - \frac{T}{\mu N r}\right)^{-1/3} \Gamma \qquad (1)$$

where

r rolling radius of roller under consideration

G shear modulus of the material

a Hertzian semiwidth of elliptical contact area (perpendicular to direction of rolling)

T applied torque

μ available traction coefficient

N normal load

Γ contact geometry parameter which depends only on Poisson's ratio and contact ellipticity ratio a/b

Alternately, the torsional stiffness k_t of a traction roller is defined as the reciprocal of the compliance (or c_t^{-1}). It can be seen from the previous equation that torsional stiffness is not linear with torque. It should be noted that compliance (or stiffness) is defined as the slope of the deflection versus torque (or torque versus deflection) curve for each particular roller contact.

Rolling Contact

The foregoing analysis treats the static case where the rollers' contact point remains fixed in space under the line of centers between the rollers' centers. The only motion is equal and opposite circumferential deflection. However, as explained in reference 11, even a simple roller pair, with a locked output shaft will see some rolling. Under certain conditions rolling motions will alter the contact torsional compliance. Thus, rolling contact effects are included in the stiffness analysis as summarized here.

In drives where one or more pairs of contacting rollers are in series with a driver and driven, there are essentially three sources of rolling motion which affect the contact torsional compliance and are superimposed on the static compliance. The first is gross rotation of the driven element. In a slewing operation, steady-state rotation and associated creep do not affect the roller contact torsional stiffness. However, in a system where torque is applied and the driven inertia accelerates from rest, the early motions can affect the contact stiffness. The second source is downstream torsional compliance. Even if the driven element is fixed so that no gross rotation occurs, the components coupling it to the roller drive will have finite stiffness. Similarly, in a multistage drive, each roller contact has a finite stiffness.

Thus, each roller contact will see the motion produced by deflections downstream. The third source of rolling motion is the rotation induced by the static compliance of the rollers themselves which causes some very small rotation. This motion tends to sweep roller surface material in and out of the contact as if it were rolling.

Two contacting bodies which are rolling with a globally steady velocity and tangential load will experience a small, relative velocity difference known as creep. This velocity difference is due to the state of the elastic strain in the surfaces as the roller material is swept through the contact region. Material is tangentially stretched and compressed, or vice versa, and the surface traction forces which locally exceed the coefficient of friction cause areas of microslip which relieve the strain without gross sliding. Creep is of great engineering importance because the product of creep and tangential force is a measure of the power loss.

Several theoretical models of creep have been proposed and evaluated. The expressions for determining the value of creep for a dry contact chosen in reference 11 were

$$\frac{\Delta U}{U} = \frac{3\mu N}{G\pi ab}(1 - \nu)(1 - K) \tag{2}$$

where

ν Poisson's ratio
b Hertzian semiminor contact width (in direction of rolling)

and

$$\frac{\Delta U}{U} = \frac{(U_1 - U_2)}{(U_1 + U_2)/2} \tag{3}$$

where

$U_{1,2}$ solid-body surface speed of rollers 1 and 2

K dimensionless measure of the locked portion of the rolling contact determined from

$$\frac{F_x}{\mu N} = 1 - \frac{3}{2}\left\{\left[2K - K^2\right]^{1/2}\left[1 - \frac{2}{3}K + \frac{1}{3}K^2\right] - (1 - K)\sin^{-1}\left[\left(2K - K^2\right)\right]^{1/2}\right\} \tag{4}$$

where

F_x tangential force in rolling direction

To calculate the motion due to rolling creep, the motion itself is desired rather than the rate of motion by which creep is normally defined. As shown

in reference 11, creep at constant torque can be expressed as angular motion θ over some small time interval Δt by

$$\frac{\Delta\theta}{\theta} = \frac{X_1/r_1 - X_2/r_2}{(X_1/r_1 + X_2/r_2)/2} \tag{5}$$

where

$X_{1,2}$ solid-body surface motion of rollers 1 and 2

$r_{1,2}$ radii of rollers 1 and 2

To utilize this analysis, loads are applied incrementally. At each small torque increment, values of K, creep rate, and angular motion are calculated for each of the simple contacts. The resultant rolling contribution is combined with the static deflection obtained in that torque increment using the principle of linear superposition. Appropriate values of motion are found using this incremental approach for each roller contact which include the effects of structural deflection.

The direct superposition of rolling and static compliance is not strictly correct since the surface stress fields and microslip regions are not the same. However, as was shown in reference 11, this method provides a reasonable approximation of roller contact stiffness, especially for positioning mechanisms which spend much of their time "hunting" for position about the zero torque crossing region.

REFERENCES

1. Bryan, J.B.: Design and Construction of An Ultraprecision 84 Inch Diamond Turning Machine. Precis. Eng., vol. 1, no. 1, Jan. 1979, pp. 13-17.

2. Steinetz, B.M., et al.: An Advanced Pitch Change Mechanism Incorporating a Hybrid Traction Drive. AIAA Paper 84-1383, June 1984.

3. Nasvytis, A.L.: Multiroller Planetary Friction Drive. SAE Paper 660763, Oct. 1966.

4. High Torque CMG Rotary Actuator. (ACS-10357, General Electric Co.;NASA Contract NAS5-20298) NASA CR-122458, 1972, p. 2-1.

5. Auclair, G.F.; and Seminski, R.B.: Roller-Gear Drive Development. (ACD-10104, General Electric Co.; NASA Contract NAS8-26213) NASA CR-103057, 1971, p. 4.

6. Spalvin, Talivaldis; and Buzek, Bruno: Frictional and Morphological Characteristics of Ion-Plated Soft Metallic Films. Thin Solid Films, vol. 84, 1981, pp. 267-272.

7. Spalvins, T.: The Structure of Ion Plated Films in Relation to Coating Properties. NASA TM-87055, 1985.

8. Roark, R.J.; and Young, W.C.: Formulas for Stress and Strain, 5th ed., McGraw-Hill, 1975.

9. Harris, T.A.: Rolling Bearing Analysis, Wiley, New York, 1966, pp. 166-171.

10. Nestorides, E.J.: A Handbook on Torsional Vibration, Cambridge University Press, Cambridge, Eng., 1958, pp. 98-99.

11. Rohn, D.A.; and Loewenthal, S.H.: An Analysis of Traction Drive Torsional Stiffness. J. Mech. Trans. Automation Des., vol. 107, no. 4, Dec. 1985, pp. 573-581.

12. Kannel, J.W.; and Dow, T.A.: Analysis of Traction Forces on a Precision Traction Drive. ASME Paper 85-TRIB-45, Oct. 1985.

13. Loewenthal, S.H.; Rohn, D.A.; and Steinetz, B.M.: Application of Traction Drives as Servo Mechanisms. Nineteenth Aerospace Mechanisms Symposium, NASA CP-2371, 1985, pp. 119-139.

14. Cornell, R.W.: Compliance and Stress Sensitivity of Spur Gear Teeth. J. Mech. Des., vol. 103, no. 2, Apr. 1981, pp. 447-459.

TABLE I. - THEORETICAL STIFFNESS (FULLY REFLECTED TO OUTPUT) OF THE TEST TRACTION ROLLER DRIVE AT ZERO TORQUE AND 50 PERCENT INITIAL PRELOAD

Element	Stiffness, N-m/rad (ft-lb/rad)	Compliance, rad/N-m (rad/ft-lb)	Percent of total compliance
Spider cage/bearing and aluminum support posts	2.00×10^{6} (1.50×10^{6})	$.50\times10^{-6}$ ($.667\times10^{-6}$)	33
Planet bearings-cylindrical roller (203) diametral clearance = 5 μm (assumed)	2.80×10^{6} (2.11×10^{6})	$.357\times10^{-6}$ ($.474\times10^{-6}$)	23
Input shaft and torque loader system (bearing balls)	3.80×10^{6} (2.79×10^{6})	$.263\times10^{-6}$ ($.358\times10^{-6}$)	18
All traction contacts ($\mu_{gold} = 0.12; \mu_{steel} = 0.2$)	7.90×10^{6} (5.80×10^{6})	$.127\times10^{-6}$ ($.172\times10^{-6}$)	9
Roller support housing backing plate (aluminum)	8.63×10^{6} (6.37×10^{6})	$.115\times10^{-6}$ ($.157\times10^{-6}$)	8
Outer housing (aluminum)	17.1×10^{6} (12.6×10^{6})	$.058\times10^{-6}$ ($.079\times10^{-6}$)	4
Bearing post depression in aluminum backing plate	19.4×10^{6} (14.30×10^{6})	$.052\times10^{-6}$ ($.070\times10^{-6}$)	3
Output shaft	29.4×10^{6} (21.7×10^{6})	$.034\times10^{-6}$ ($.046\times10^{-6}$)	2
Total drive	$.670\times10^{6}$ ($.494\times10^{6}$)	1.506×10^{-6} (2.023×10^{-6})	100

TABLE II. - COMPARISON OF PREDICTED AND MEASURED STIFFNESSES (FULLY REFLECTED TO OUTPUT)

Element	Predicted stiffness, N-m/rad (ft-lb/rad)	Measured stiffness, N-m/rad (ft-lb/rad)
Spider cage-bearing and aluminum support posts	2.00×10^6 (1.50×10^6)	$.99 \times 10^6$ ($.730 \times 10^6$)
Planet bearings- cylindrical roller (203) diametral clearance = 5 μm (assumed)	2.80×10^6 (2.10×10^6)	$.770 \times 10^6$ ($.570 \times 10^6$)
Total drive	$.670 \times 10^6$ ($.494 \times 10^6$)	$.230 \times 10^6$ ($.170 \times 10^6$)
Total drive[a]	$.370 \times 10^6$ ($.270 \times 10^6$)	----------
Total drive[b]	$.230 \times 10^6$ ($.170 \times 10^6$)	----------

[a]Drive stiffness recalculated based on the measured planet bearing and spider cage component stiffnesses.
[b]Drive stiffness recalculated based on measured planet bearing and spider cage component stiffnesses assuming nonideal load sharing of second-row planet bearings.

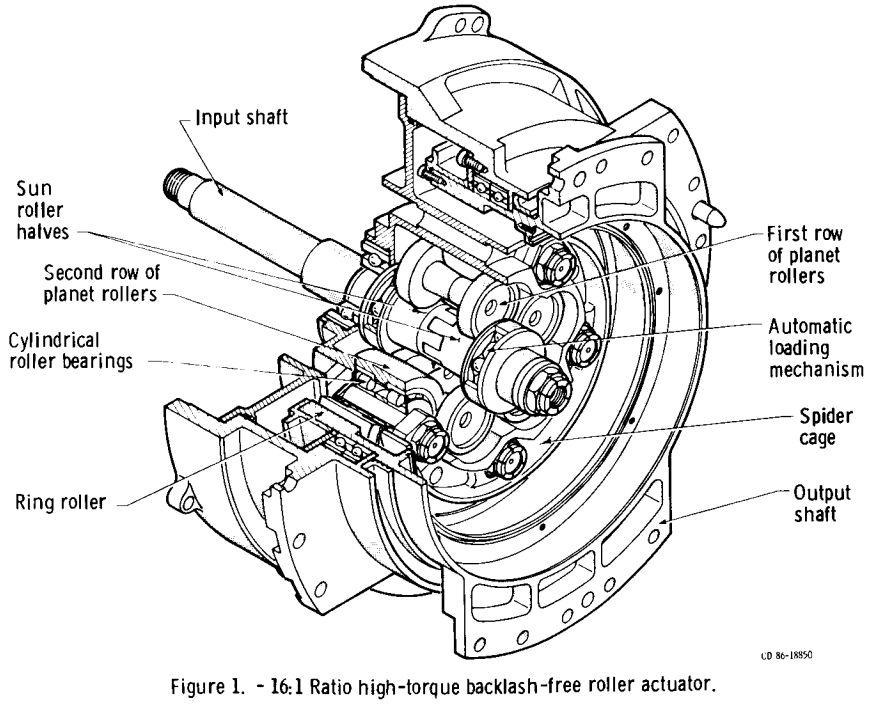

Figure 1. - 16:1 Ratio high-torque backlash-free roller actuator.

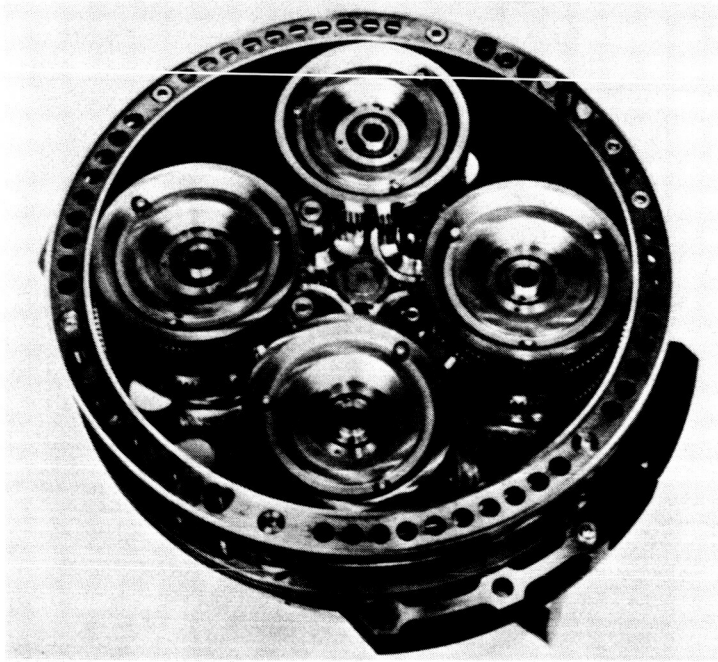

Figure 2. - 26: 1 ratio control moment gyro roller gear drive.

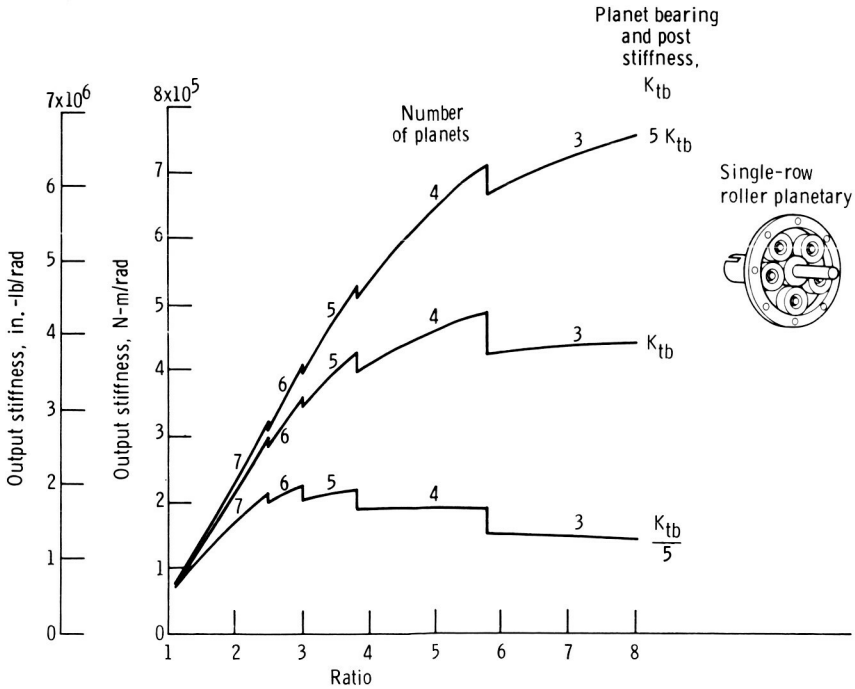

Figure 3. - Maximum torsional stiffness of single-row roller planetary as a function of ratio. Output torque, traction coefficient, contact ellipticity, ring diameter, and input and output shaft stiffnesses are constant. The number of planets is limited by planet-to-planet interference.

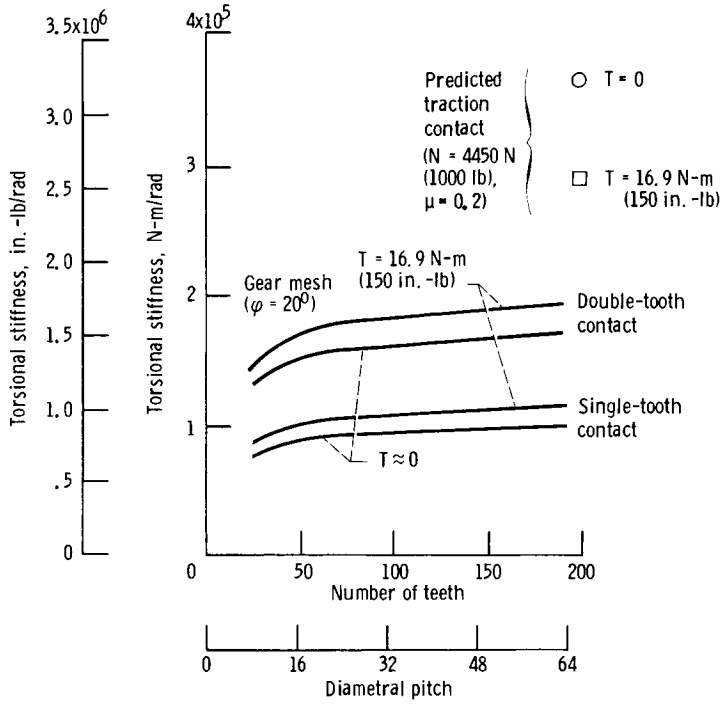

Figure 4. - Theoretical comparison of gear mesh and traction roller contact torsional stiffness at equal diameters, 76.2 mm (3.0 in.), widths, 4.57 mm (0.18 in.), and loads (ref. 13).

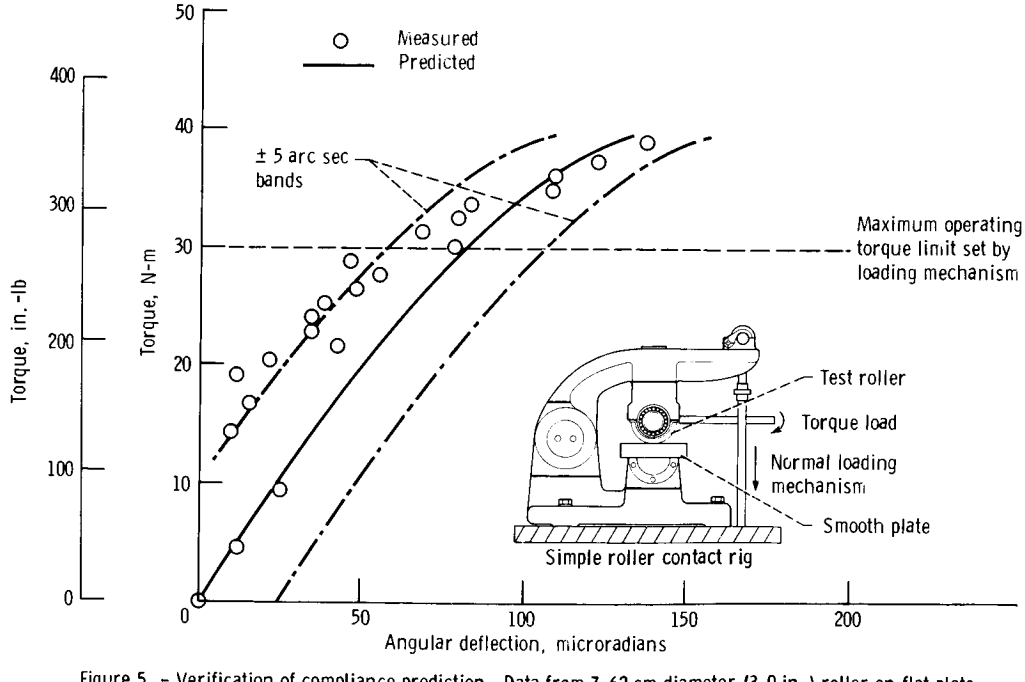

Figure 5. - Verification of compliance prediction. Data from 7.62 cm diameter (3.0 in.) roller on flat plate. Ellipticity ratio, 4.3; available traction coefficient, 0.24; normal force, 4450 N (1000 lb).

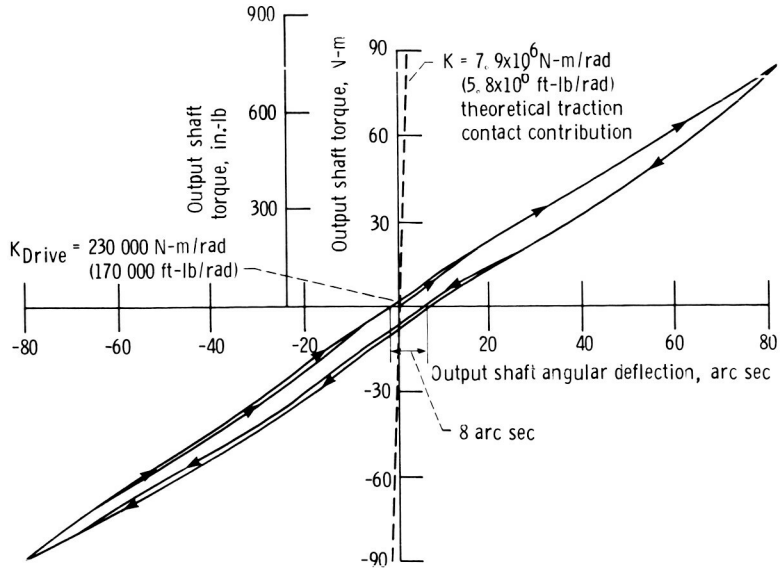

Figure 6. - Roller drive output shaft torque versus output shaft angular deflection. Sun input shaft locked; roller normal loads, 50 percent of maximum; data shown are for two full cycles of positive and negative torque.

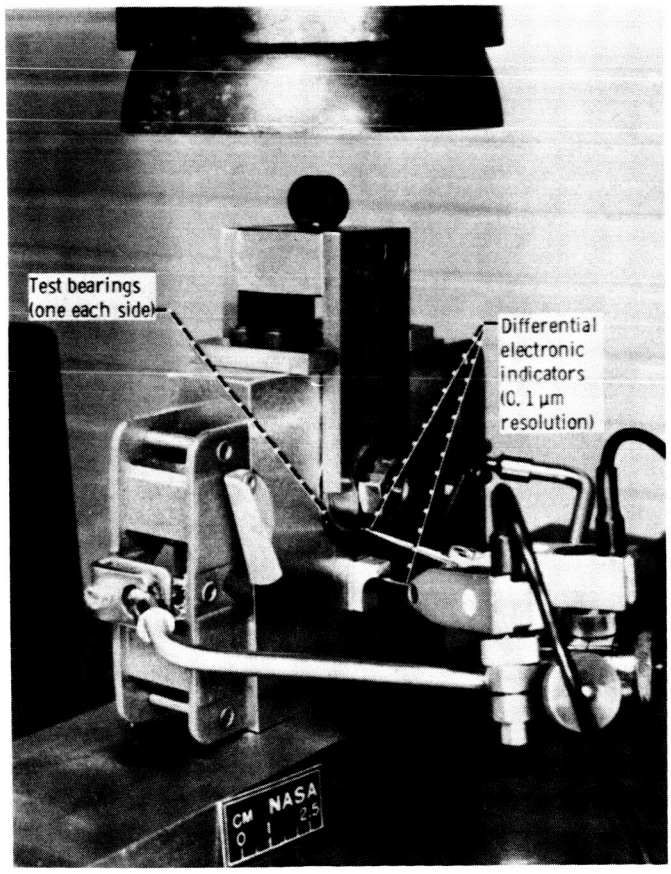

Figure 7. - Roller bearing radial stiffness test fixture.

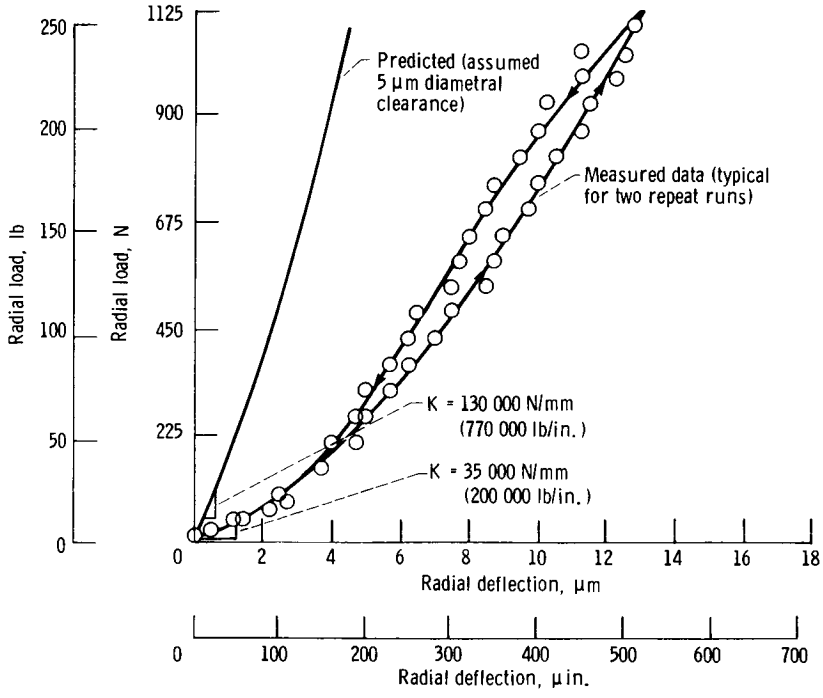

Figure 8. - Comparison of measured and predicted (using ref. 9) load-deflection characteristics for planet roller bearing. (All bearing clearance removed before taking readings.)

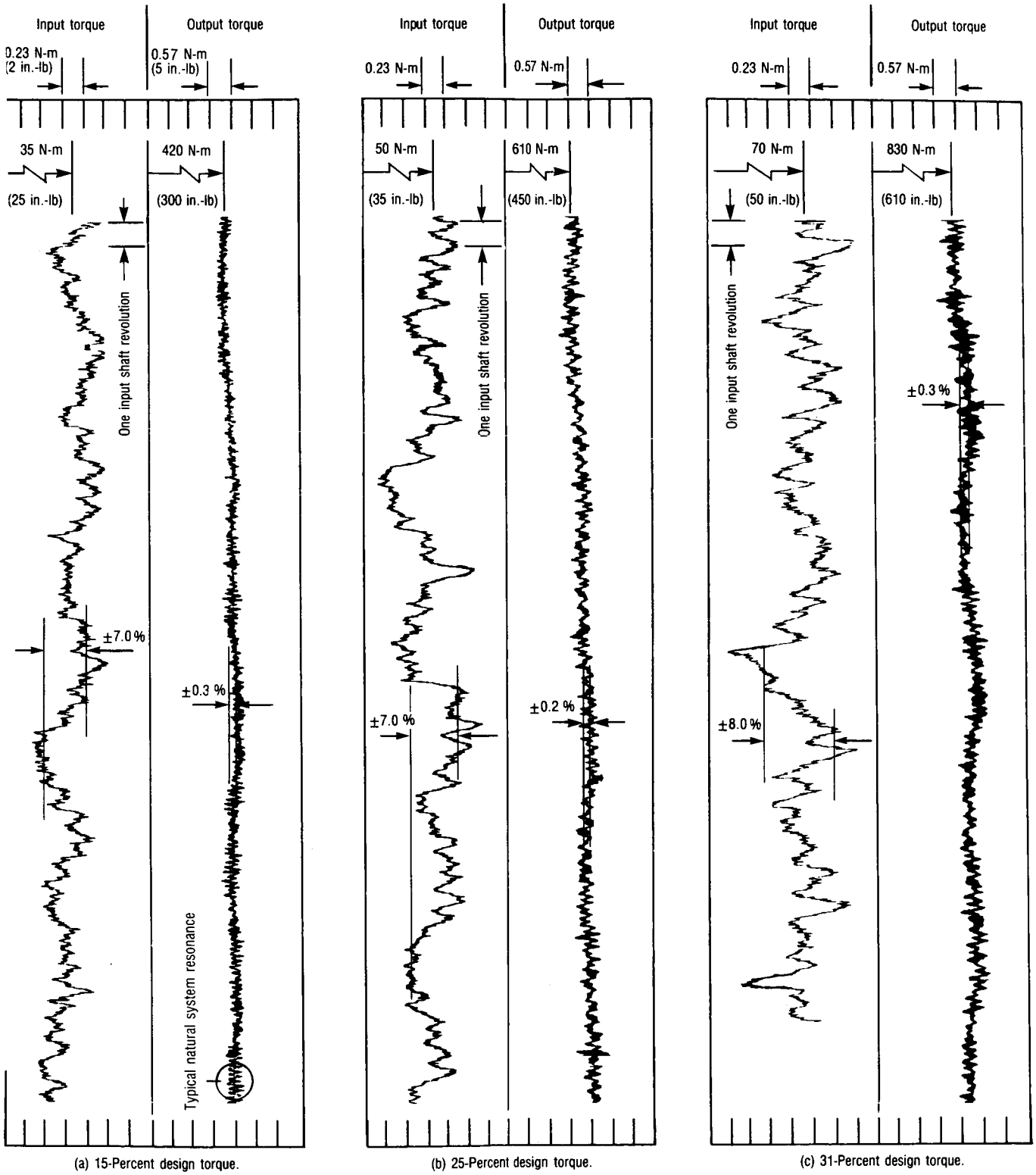

(a) 15-Percent design torque.

(b) 25-Percent design torque.

(c) 31-Percent design torque.

Figure 9. - Effect of torque on roller actuator torque signatures at input speed of 28 rpm. One full output shaft revolution shown for each torque; one input shaft revolution as indicated.

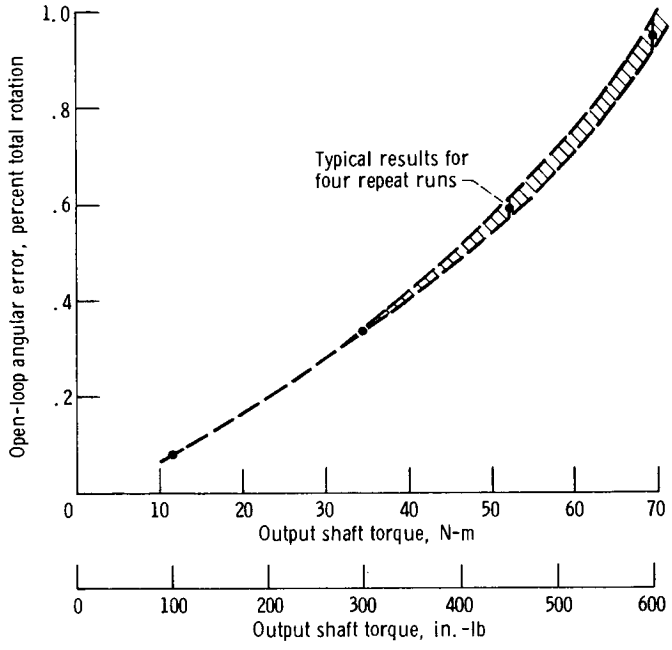

Figure 10. - Open-loop positional accuracy of roller actuator as percentage of total rotation.

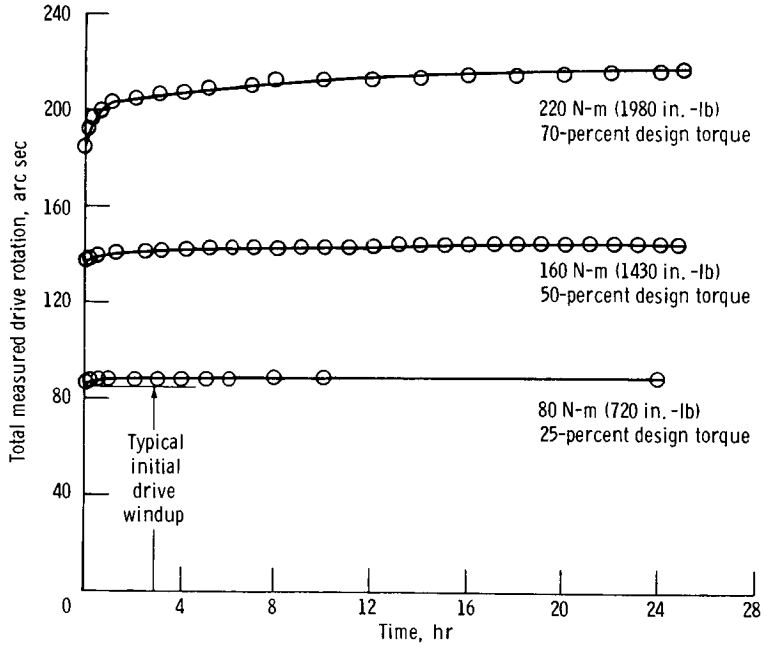

Figure 11. - Roller actuator long-term holding ability as function of percent maximum design torque. Input shaft locked; roller normal loads, 75 percent of maximum.

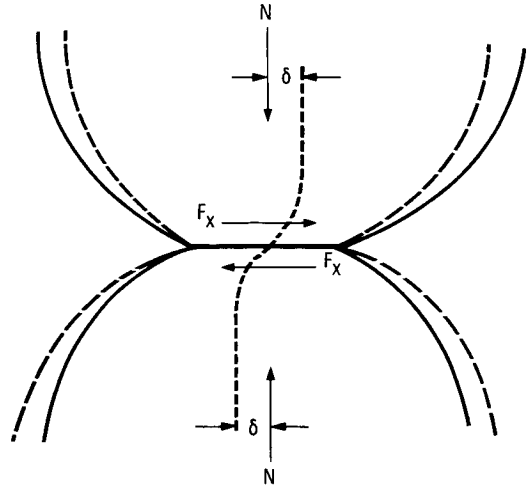

Figure 12. - Tangential deflection δ of bodies in contact under combined normal N and tangential F_x loads.